Supplementary Figures

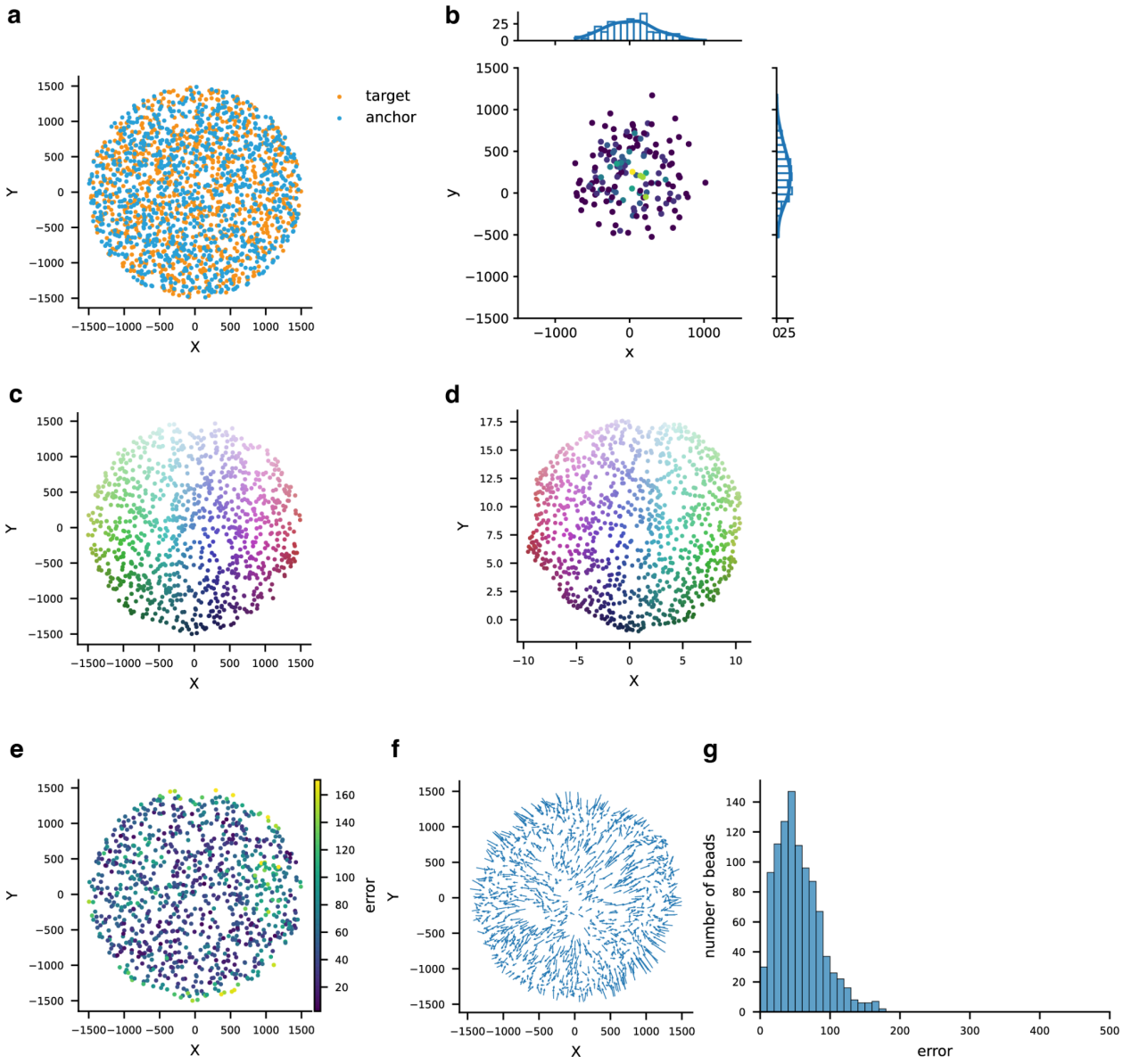

Supplemental Figure 1: Simulation of diffusion and reconstruction with UMAP
a, Simulated locations of capture beads and fiducial beads in a 3 mm circle. **b**, Simulated diffusion pattern of a capture bead on its associated fiducial beads, colored by simulated UMI counts. The distribution plots on the top and right represents the diffusion distribution on the x and y axis respectively. **c**, Simulated locations of capture beads, colored by a two dimensional color gradient depending on the locations. **d**, UMAP reconstructed locations of capture beads, colored the same as in c. **e**, Absolute error of capture beads plotted in ground truth locations. **f**, Displacement vectors of capture beads. Each arrow starts from the capture bead's ground truth location and ends at the reconstruction location. **g**, Histogram plot of capture beads' absolute error.

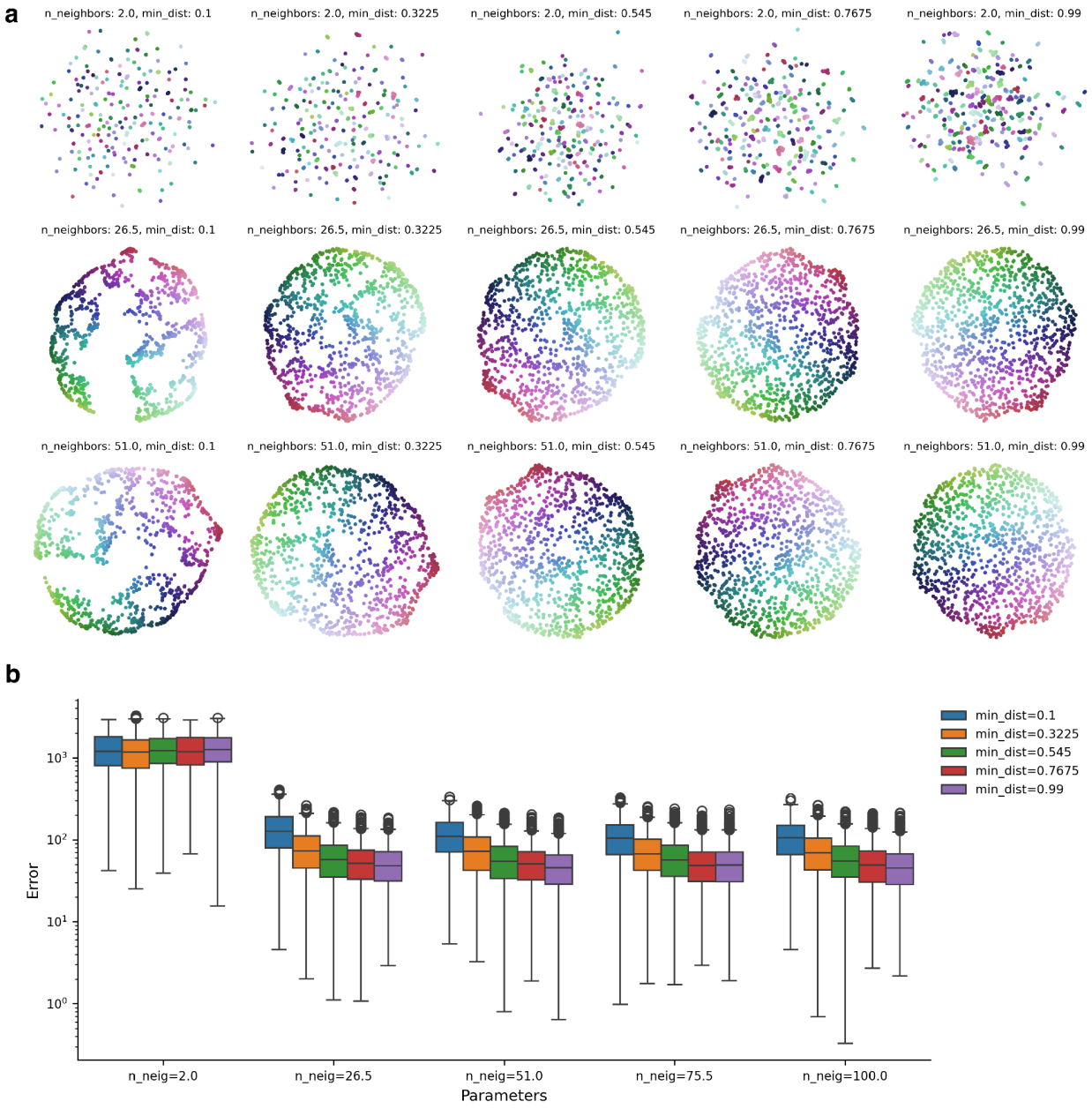

Supplemental Figure 2: UMAP parameters' effect on reconstruction

a, The same diffusion matrix is embedded in the two dimensional space with different parameters of UMAP: n_neighbors as the size of local neighborhood and min_dist as effective minimum distance between embedded points[16]. Each bead is colored the same as in Supplemental Figure 1.c to show the pattern recovery. **b**, Boxplot of reconstruction error with different UMAP parameters. Each box represents absolute errors of beads with corresponding parameters, with middle box as error between 25% to 75%, middle line as median error, and outlier as 1.5 times of interquartile range (IQR).

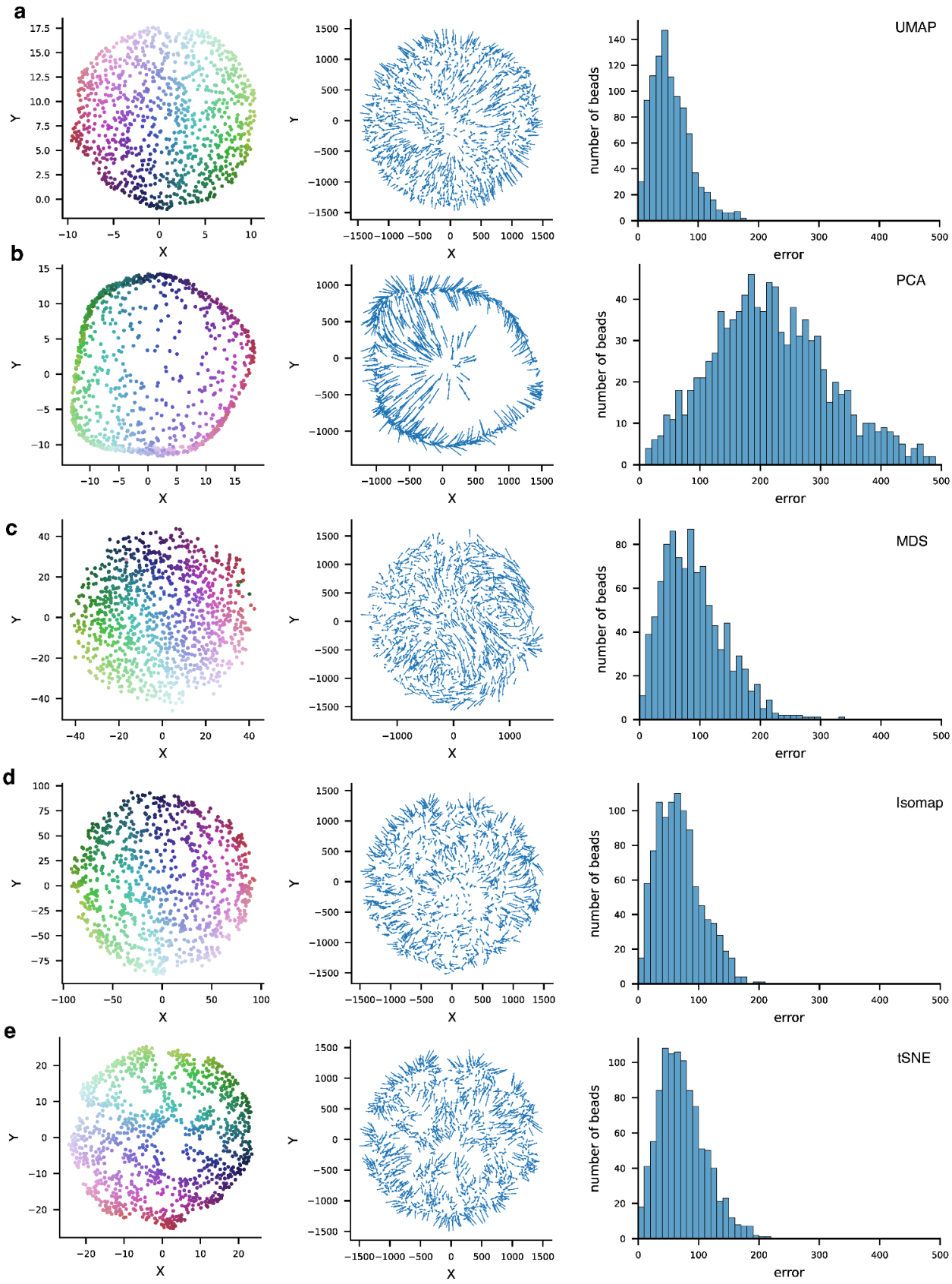

Supplemental Figure 3: Reconstruction with different dimensionality reduction methods
Reconstruction of identical simulation data with **a**, UMAP, same as Supplementary Fig1. **b**, Principal component analysis (PCA). **c**, Multidimensional scaling (MDS). **d**, Isomap. **e**, t-distributed stochastic neighbor embedding (t-SNE). Columns: Left, Reconstructed locations of capture beads, colored the same as in Supplemental Figure 1.c. Middle, Displacement vectors of capture beads. Each arrow starts from the capture bead's ground truth location and ends at the reconstruction location. Right, Histogram plot of capture beads' absolute error.

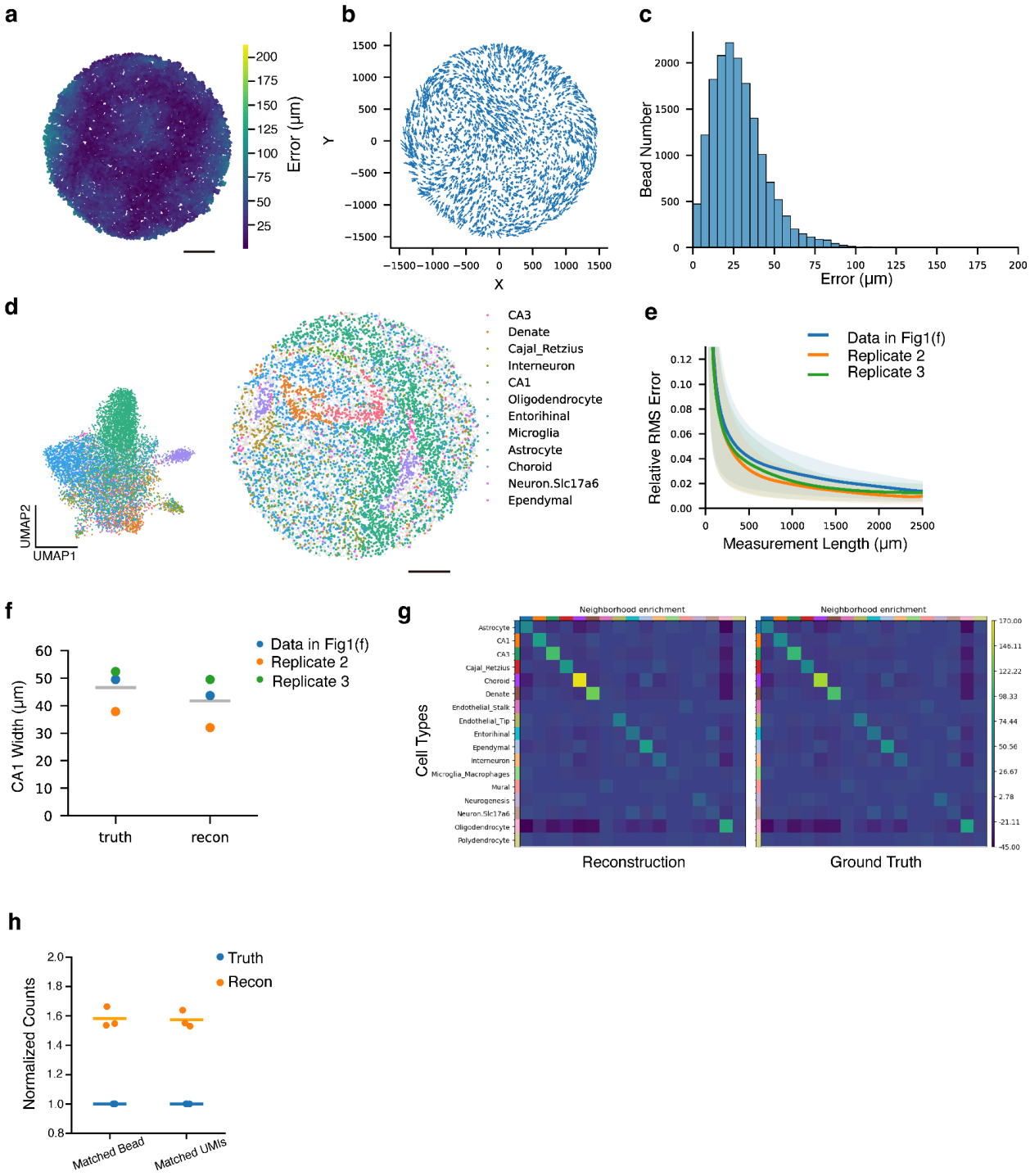

Supplemental Figure 4: Slide-seq reconstruction metrics

a, Absolute error of capture beads plotted in ground truth locations. **b**, Displacement vectors of capture beads. Each arrow starts from the capture bead's ground truth location and ends at the reconstruction location. **c**, Histogram plot of capture beads' absolute errors. **d**, (Left) UMAP representing gene expression from a coronal mouse hippocampus section captured by beads, colored by decomposed cell types from RCTD. (Right) Spatial location of capture beads in ground truth, colored by decomposed cell types. **e**, Relative RMS error of measurement lengths

as a function of measurement length. Data shown in Fig.1f (blue) and two biological replicates (orange and green) are presented. Solid lines represent average values across beads and shaded areas represent one standard deviation. **f**, CA1 width measured in ground truth and reconstruction (N = 3 biological replicates). Data shown in Fig.1f (blue) and two biological replicates (orange and green) are shown. Gray lines showed the mean width of each group. **g**, Neighborhood enrichment analysis between cell type pairs in reconstruction (left) and ground truth (right). The enrichment scores are plotted in the same color scale, higher scores represent more enriched in the neighborhoods. **h**, Comparison of matched bead barcodes and unique RNA molecules (UMIs) in reconstruction (orange) or ground truth (blue) (N = 3 biological replicates). Solid lines: mean values. Values are normalized to the ground truth for direct comparison across replicates. Scale bars: 500 μm.

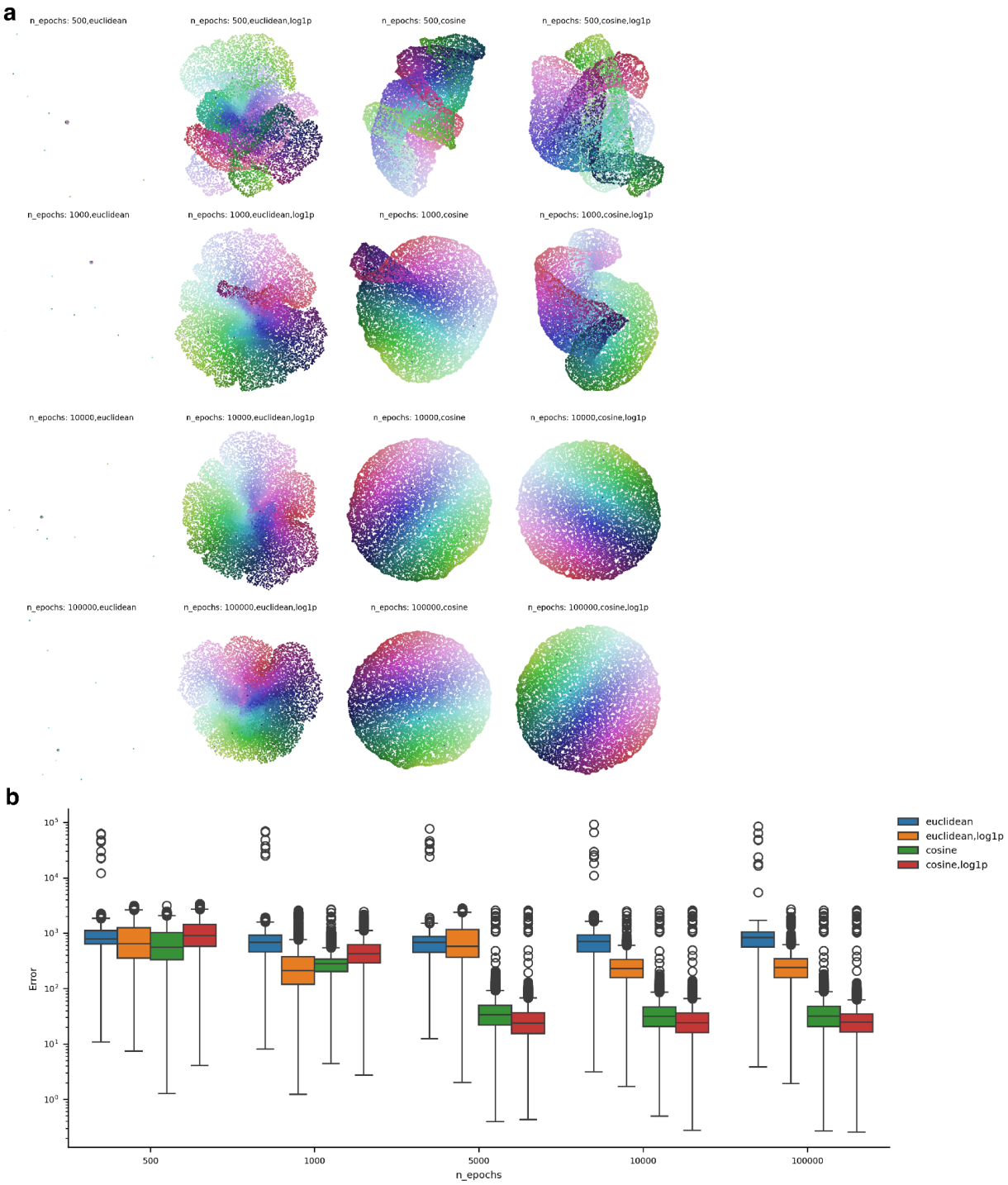

Supplemental Figure 5: UMAP parameters and matrix normalization effect on reconstruction on experimental data

a, The same diffusion matrix is embedded in the two dimensional space with different parameters of UMAP: n_epochs as the number of training epochs and metric as ways of computing distances in high dimensional space[16]. We also tested the effect of applying log1p transformation before UMAP embedding. Each bead is colored according to ground truth

location to show the pattern recovery. **b**, Boxplot of reconstruction error with different UMAP parameters and log1p transformation. Each box represents absolute errors of beads with corresponding parameters, with middle box as error between 25% to 75%, middle line as median error, and outlier as 1.5 times of interquartile range (IQR).

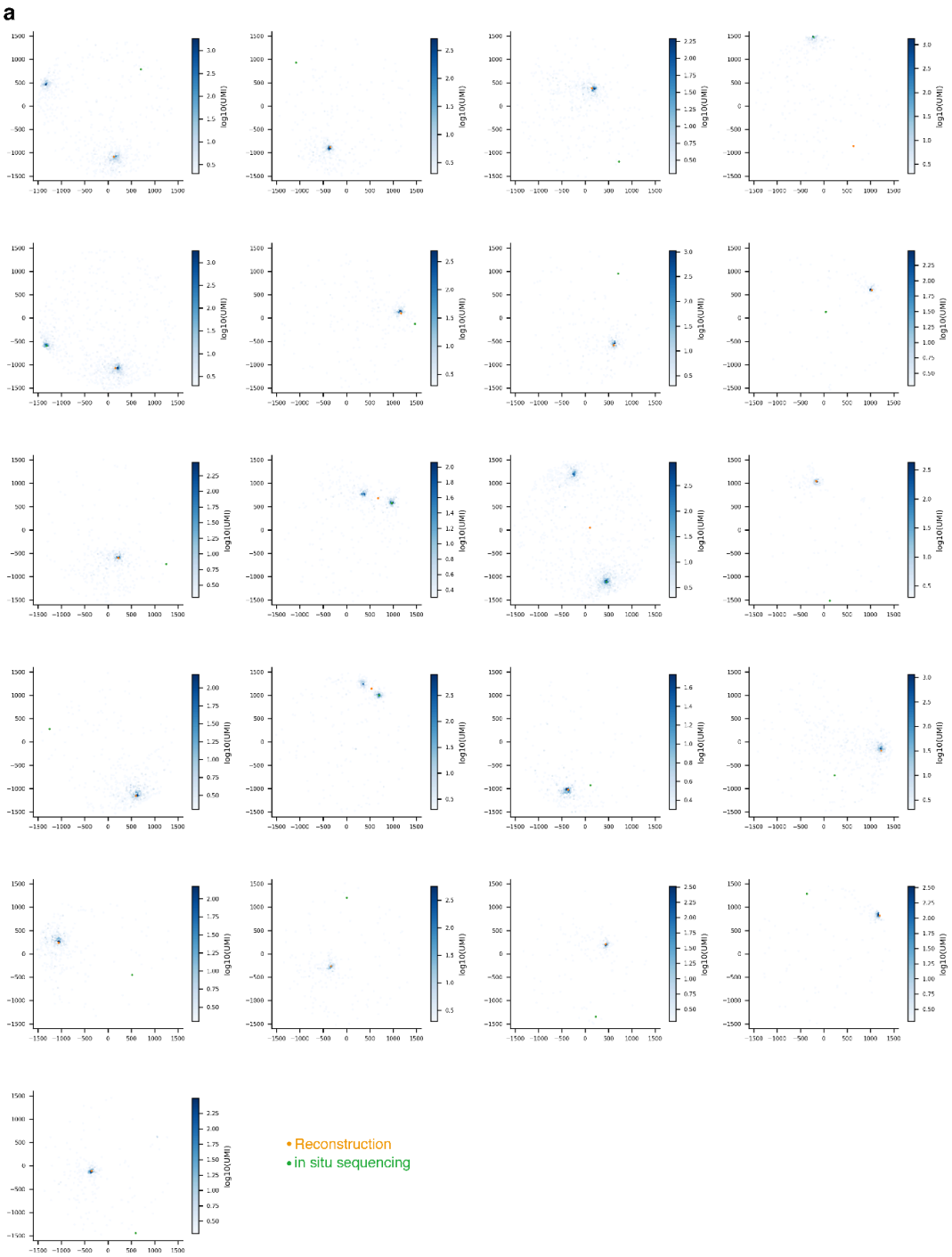

Supplemental Figure 6: Diffusion and locations of all distant (>200 μm) positioned beads
a, 21 capture beads with absolute error >200 μm are displayed with diffusion distributions (blue gradients), reconstruction locations (yellow dots), and in situ sequencing locations (green dots). Among the 21 beads, 5 beads are displayed as doublets (barcode collisions, expected from length of barcode and number of beads), 15 beads have in situ sequencing locations far away

from diffusion distribution (we anticipate these to be likely in situ sequencing error, or illumina sequencing error), and one bead has reconstruction location far away from diffusion distribution.

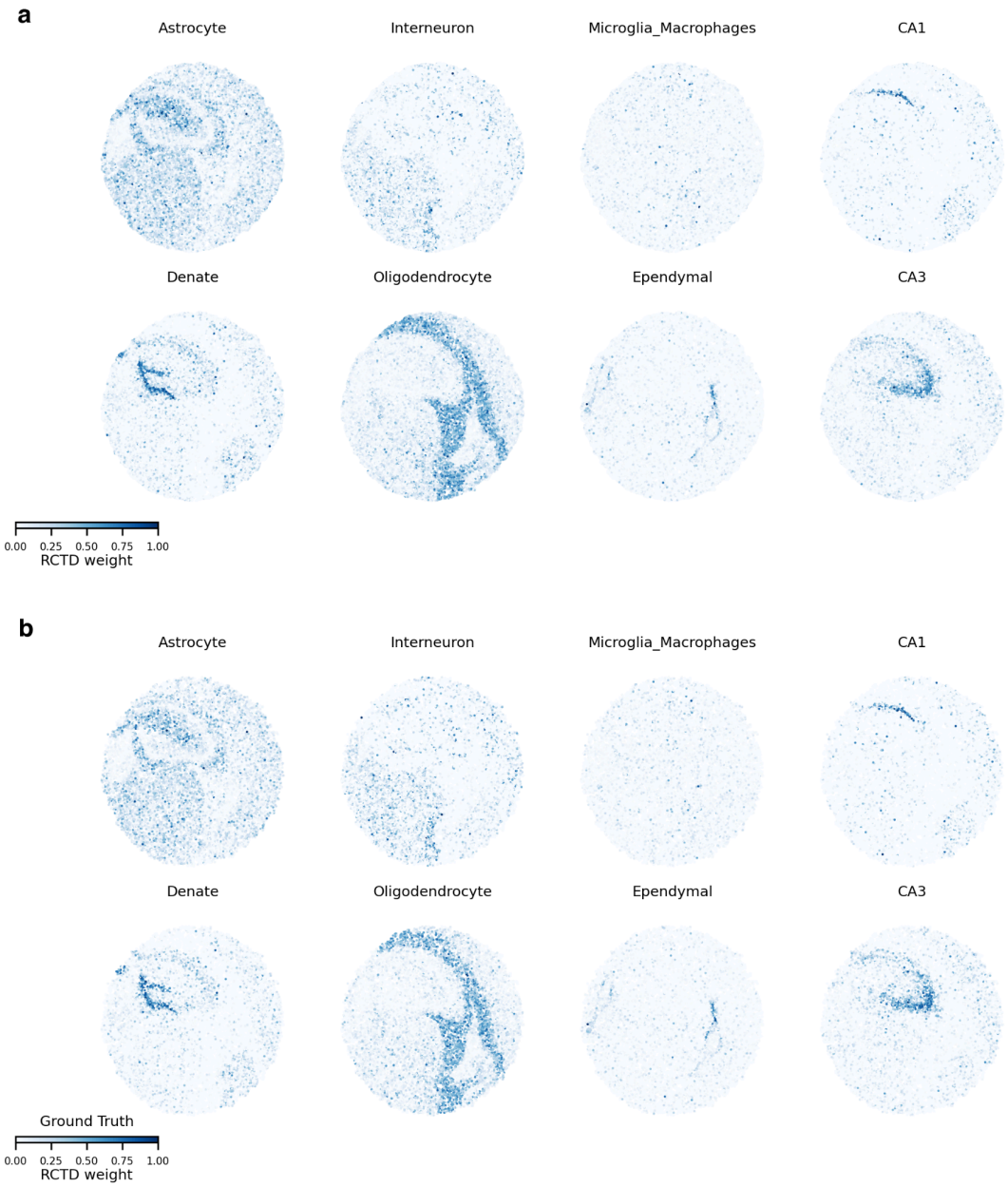

Supplemental Figure 7: Spatial distribution of cell type RCTD weights in reconstruction and ground truth

Spatial representation of RCTD inferred cell type weights in **a**, Reconstruction. **b**, Ground truth.

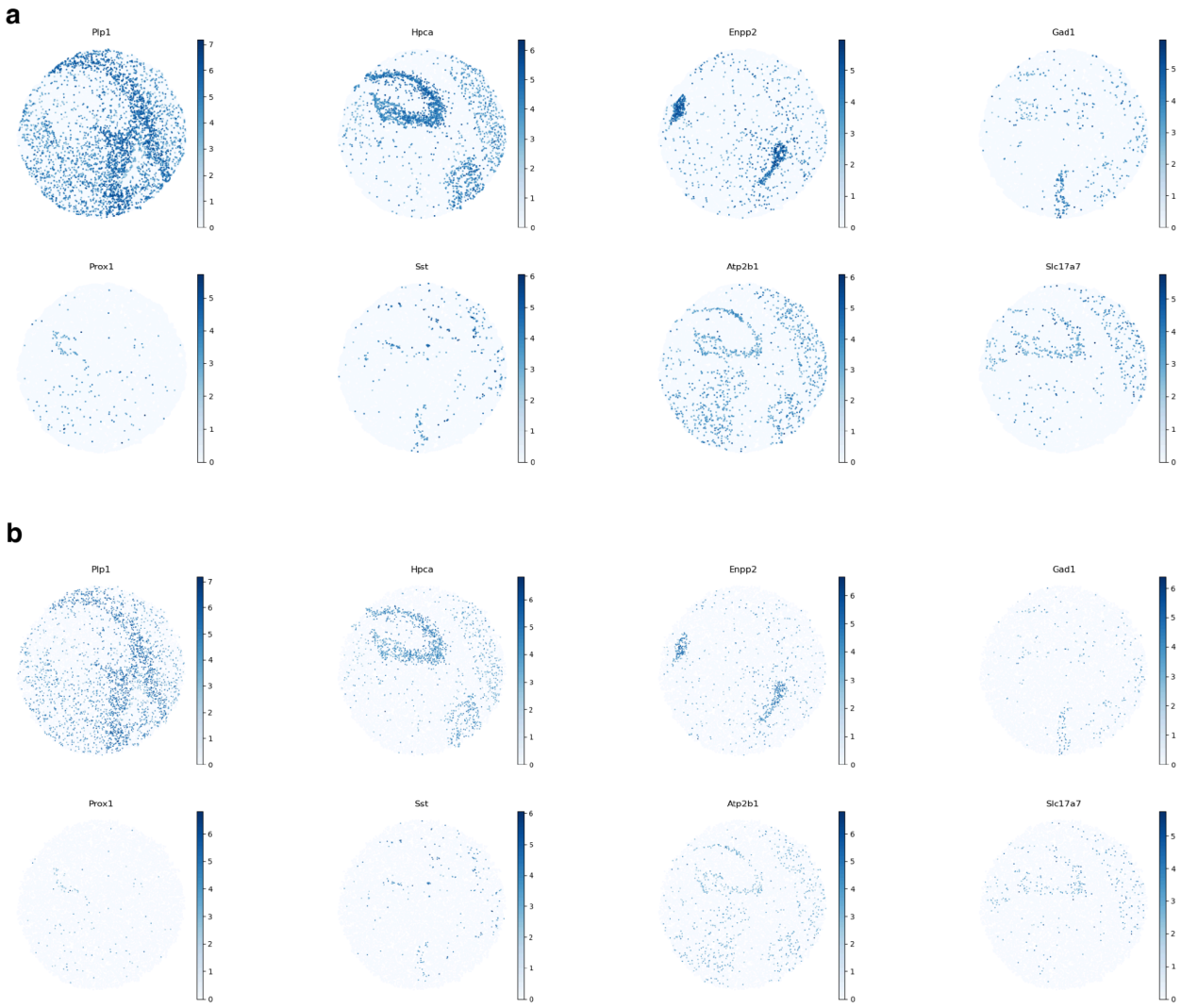

Supplemental Figure 8: Spatial distribution of genes in reconstruction and ground truth
Spatial expression pattern of marker genes in **a**, Reconstruction. **b**, Ground truth.

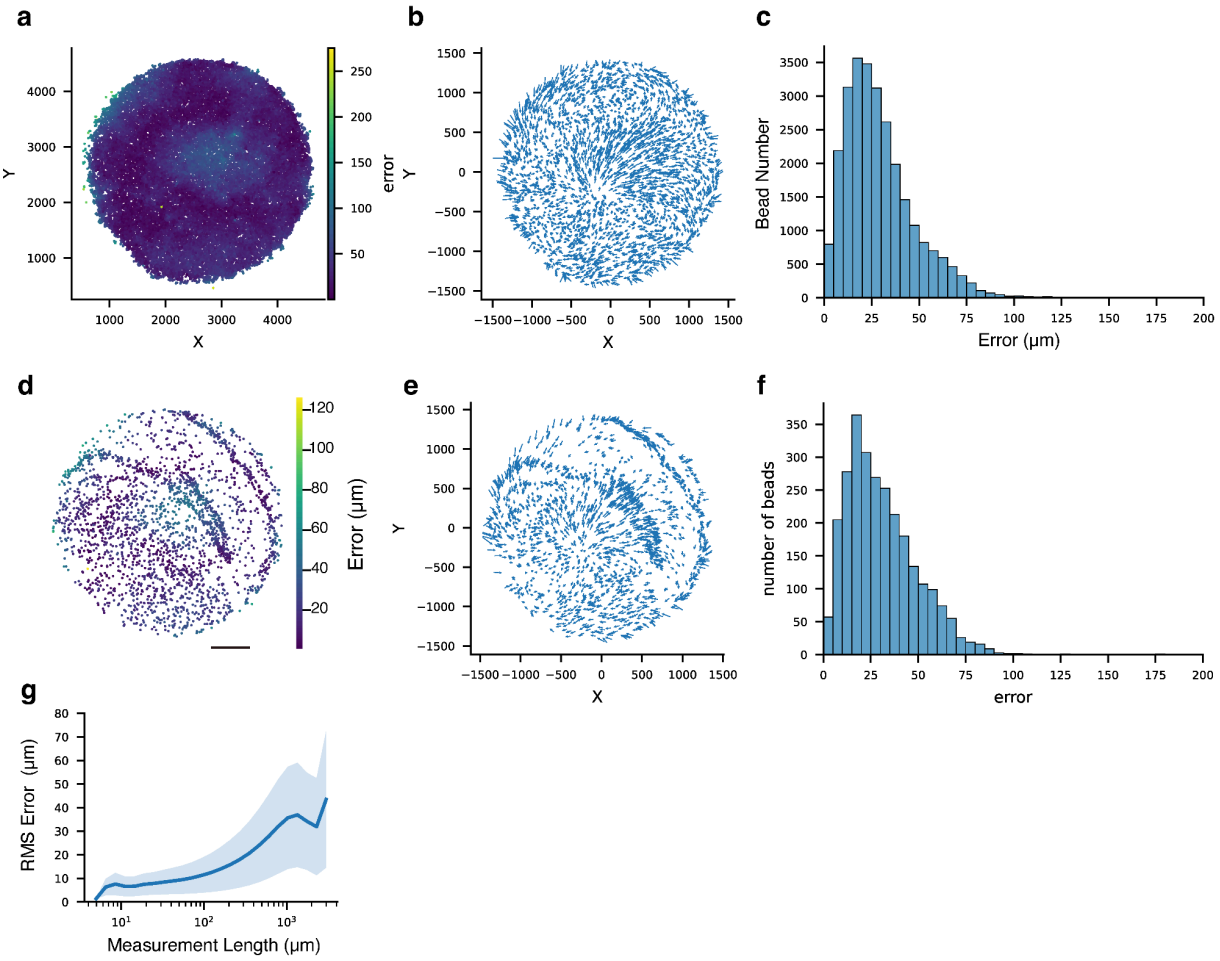

Supplemental Figure 9: Slide-tags Reconstruction metrics

a, Absolute error of capture beads plotted in ground truth locations. **b**, Displacement vectors of capture beads. Each arrow starts from the capture bead's ground truth location and ends at the reconstruction location. **c**, Histogram plot of capture bead locations' absolute errors. **d**, Spatial representation of reconstruction error on each nuclei. **e**, Displacement vectors of located nuclei. Each arrow starts from the nuclei's ground truth location and ends at the reconstruction location. **f**, Histogram plot of nuclei locations' absolute errors. **f**, RMS error of measurement lengths between bead pairs as a function of measurement length. Solid lines represent average values and shaded areas represent one standard deviation.

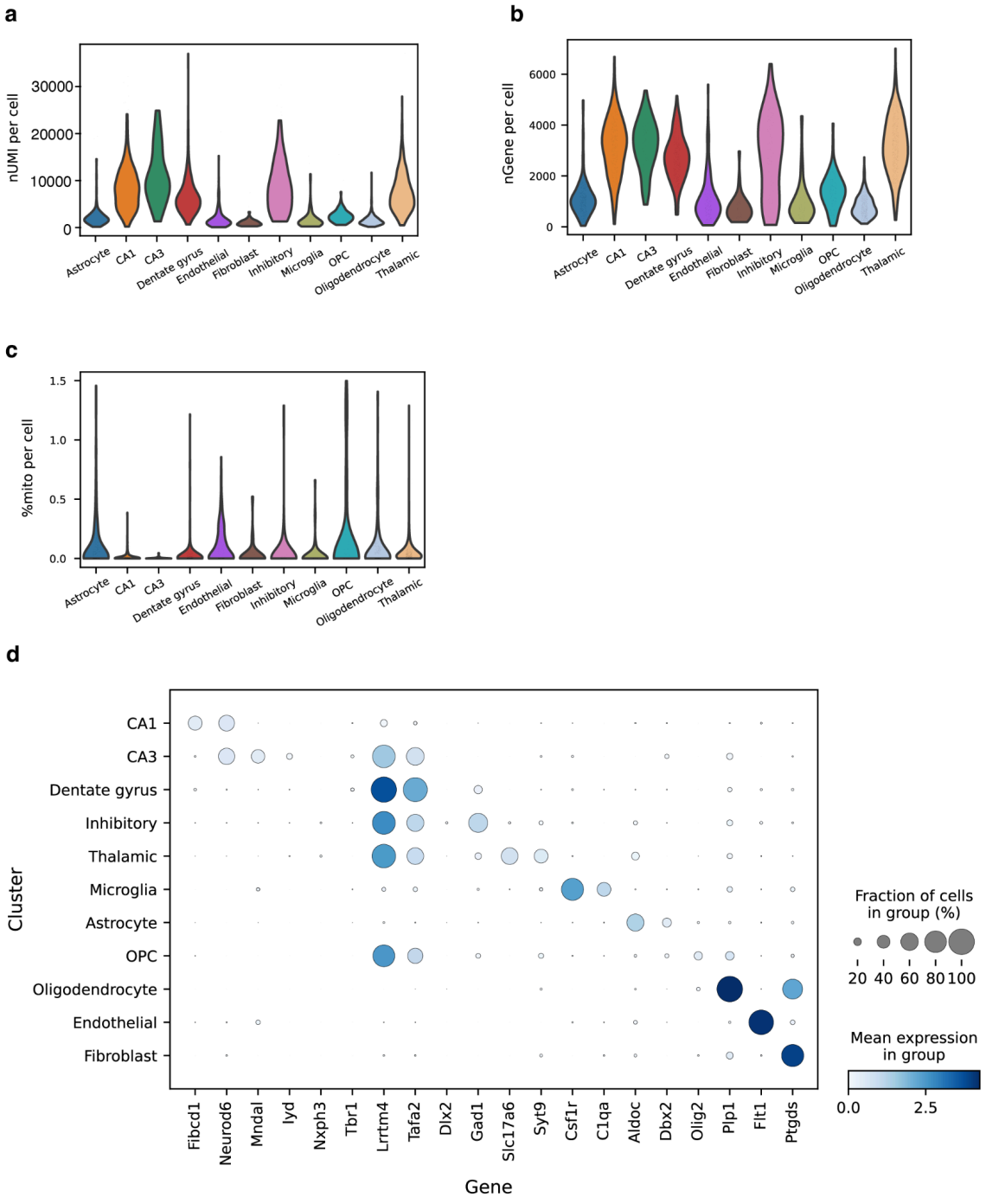

Supplemental Figure 10: snRNA-seq data metrics for Slide-tags reconstruction

a, Distribution of the number of UMI per cell for each cluster. **b**, Distribution of the number of genes per cell for each cluster. **c**, Distribution of the percentage of mitochondrial genes per cell for each cluster. **d**, Expression of marker genes by cell type cluster.

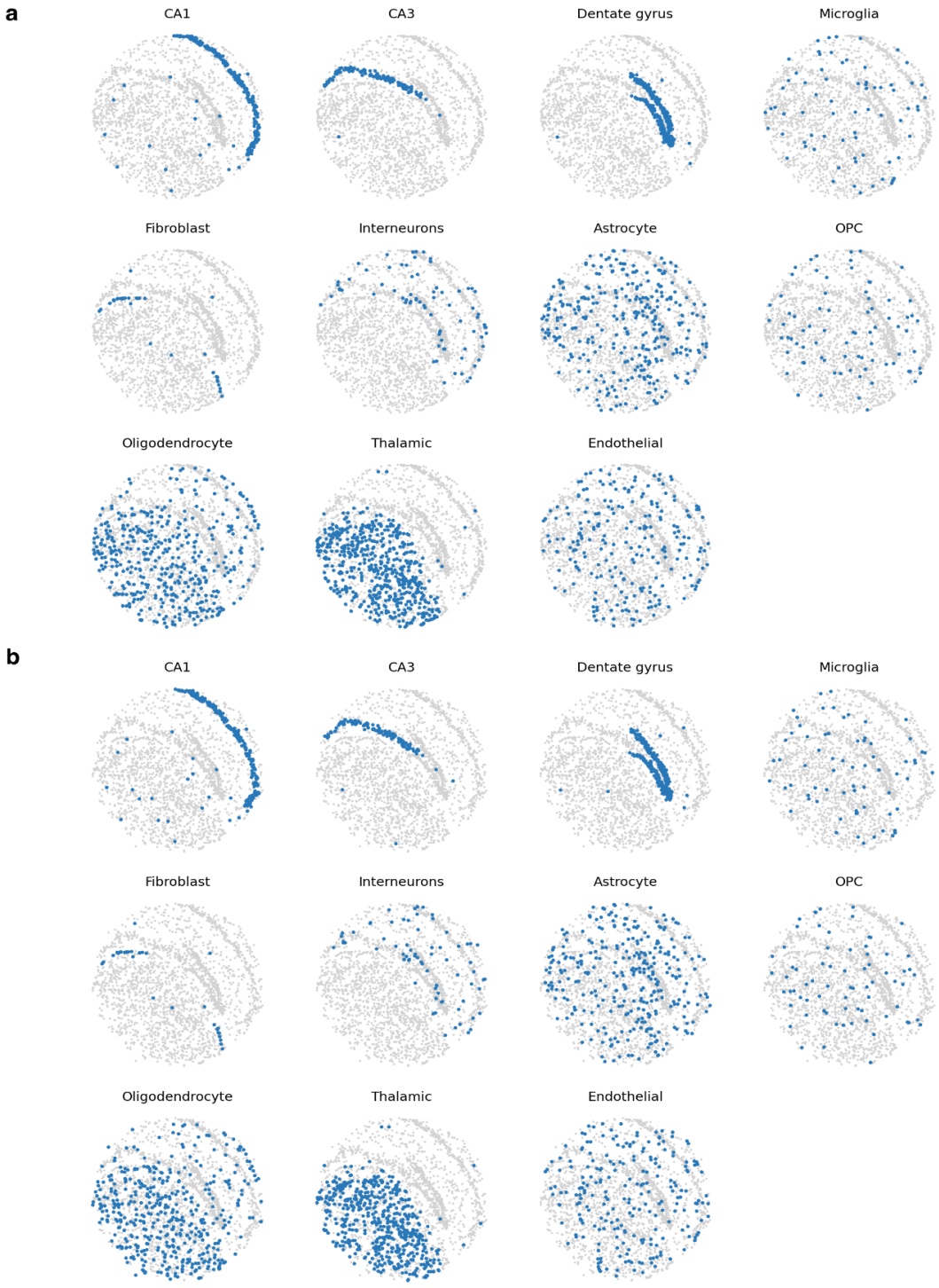

Supplemental Figure 11: Spatial representation of cell types in reconstruction and ground truth.

Spatial distribution of located cell types in **a**, Reconstruction. **b**, Ground truth.

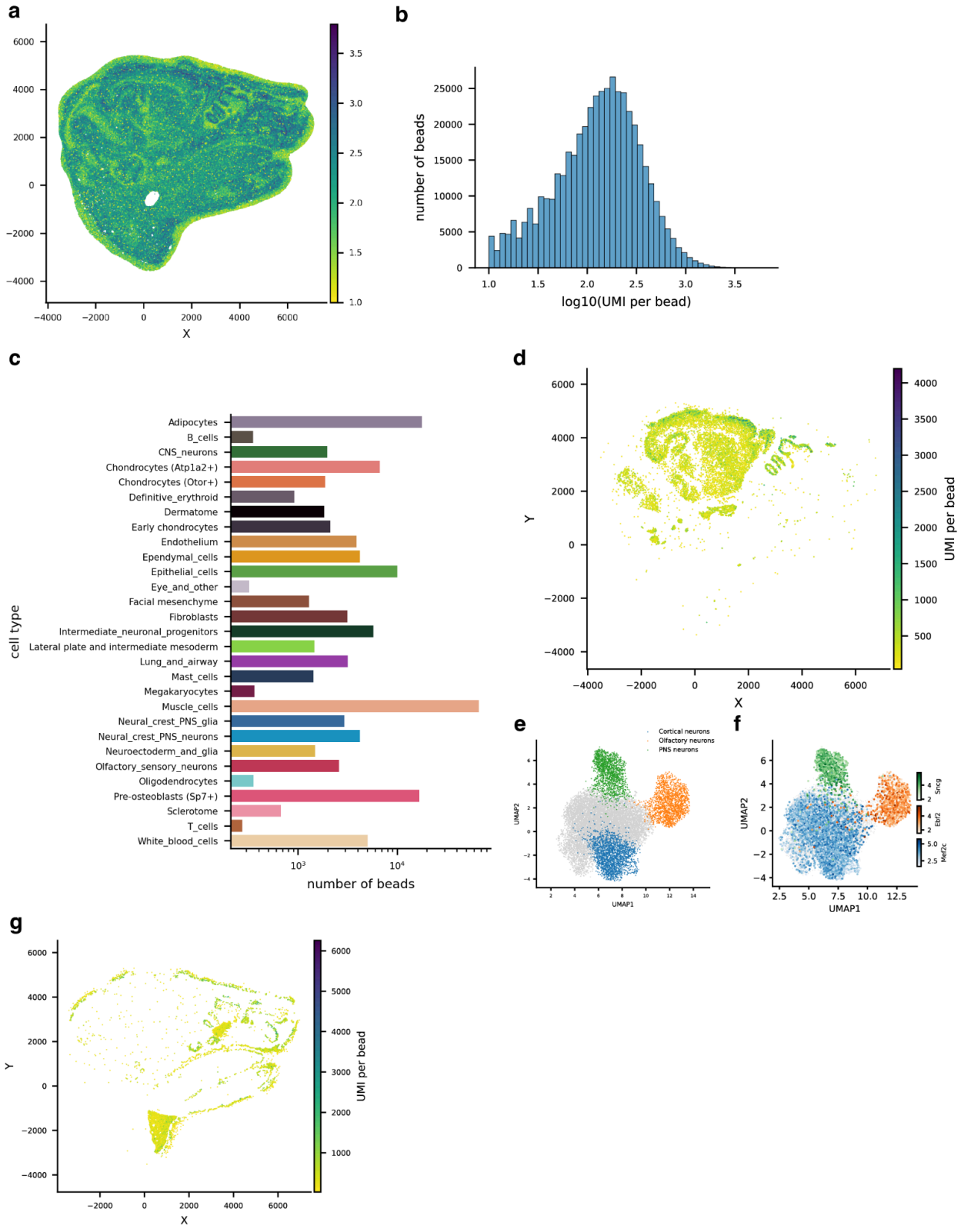

Supplemental Figure 12: Slide-seq Reconstruction for P1 mouse sample.

a, Spatial representation of UMI per bead on reconstructed locations. **b**, Distribution of UMI per bead. **c**, Number of beads with assigned cell type from RCTD. d, Spatial representation of UMI per bead of beads assigned as neuronal cells. **e**, UMAP embedding of re-clustered neuronal cells with some cell types labeled. **f**, Marker gene expression of labeled cell types in e on UMAP embedding. **g**, Spatial representation of UMI per bead of beads assigned as epithelial cells.

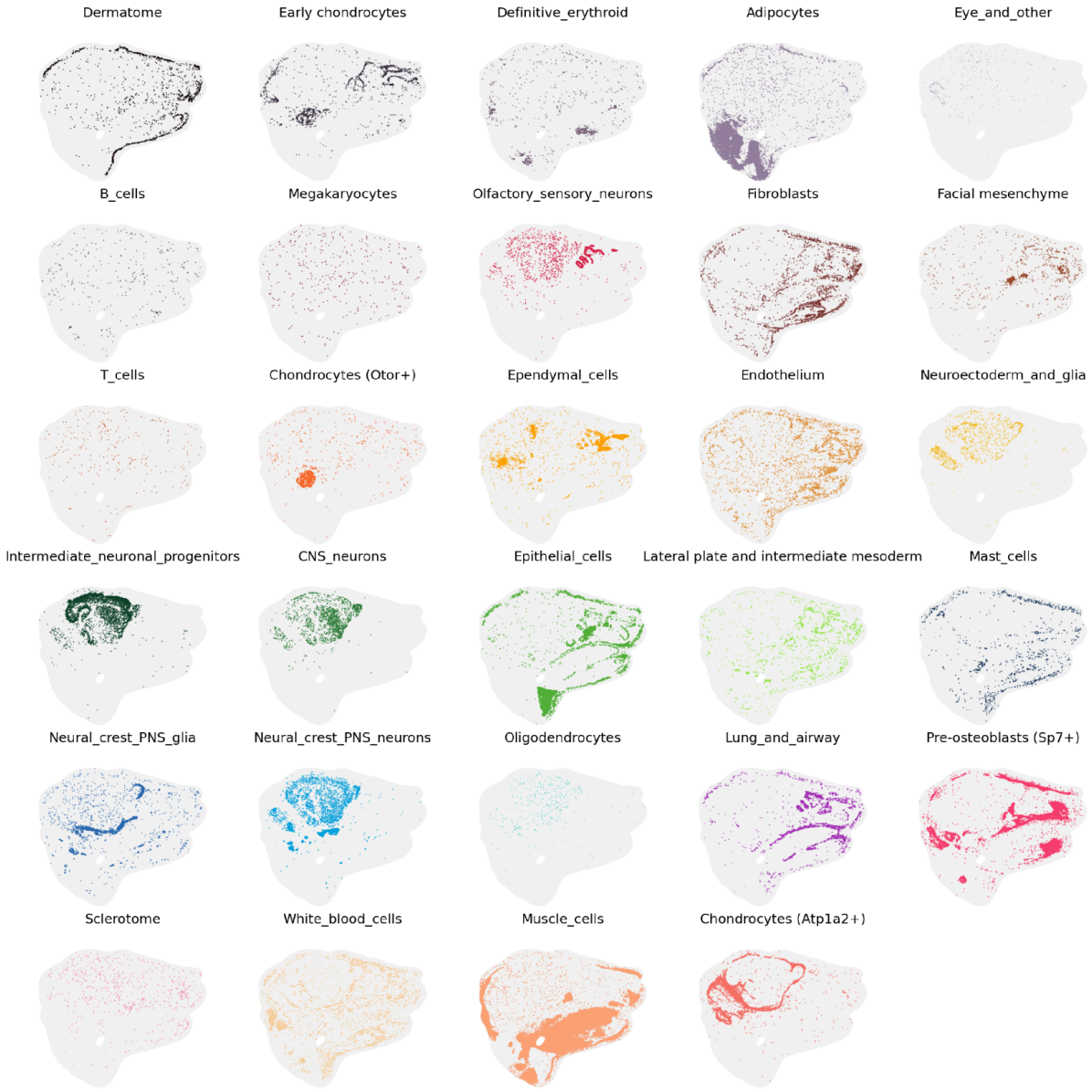

Supplemental Figure 13: Spatial representation of cell types in reconstruction of P1 mouse sample

Spatial distribution of cell types from RCTD.

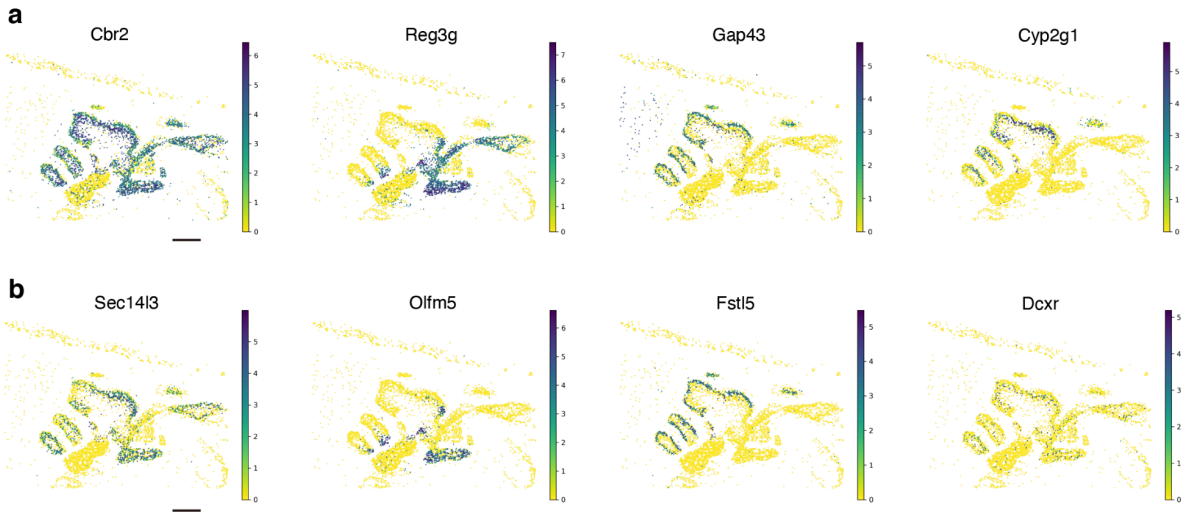

Supplemental Figure 14: Spatially differential expression genes in olfactory epithelium and respiratory epithelium

a, Spatial representation of previously characterized olfactory and respiratory differential expression genes. **b**, Spatial representation of another four less well characterized olfactory and respiratory differential expression genes that were found in this spatial data. Scale bars: 500 μm.

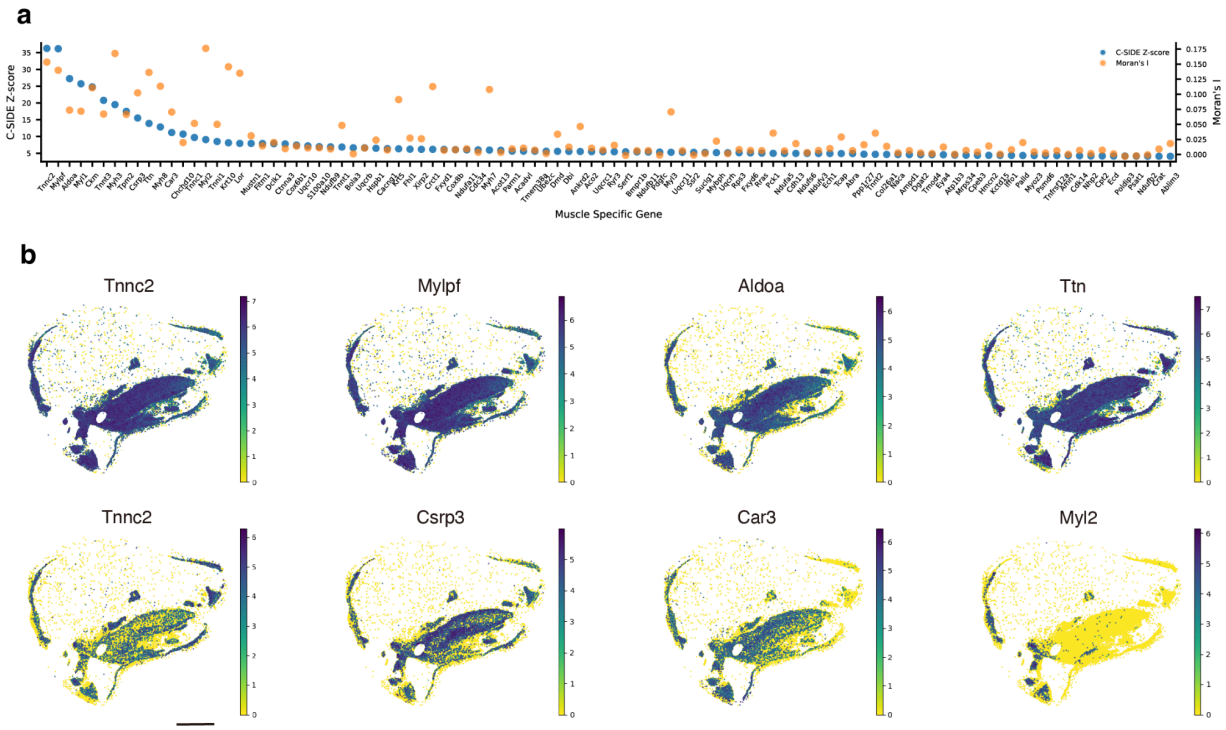

Supplemental Figure 15: Spatially differential expression genes in muscle cells

a, Top 100 spatially differential expression genes of muscle cells were ranked by nonparametric C-SIDE Z-score, with Moran'sI statistics calculated. Higher scores on both metrics signify more spatially variable expression. **b**, Spatial representation of eight spatially differential expression genes of muscle cells from b. All beads of epithelial type are positioned, colored by relative expression level of each gene. Scale bar: 2 mm.